Biochemical and Biophysical Research Communications 783 (2025) 152542

Contents lists available at ScienceDirect

Biochemical and Biophysical Research Communications

journal homepage: www.elsevier.com/locate/ybbrc

Superparamagnetic iron oxide nanoparticles – From synthesis to nanomedicine

He Wei [b], Moungi G. Bawendi [a,*]

[a] Department of Chemistry, Massachusetts Institute of Technology, 77 Massachusetts Ave, Cambridge, MA, 02139, USA
[b] Department of Chemistry and Biochemistry, California State University Fresno, 2555 E San Ramon Ave, Fresno, CA, 93740, USA

A B S T R A C T

Superparamagnetic iron oxide nanoparticles (SPIONs) have emerged as powerful tools in nanomedicine owing to their heavy-metal-free composition, distinct magnetic properties, biocompatibility, and customizable surface chemistry. While traditionally employed as T_2-weighted MRI contrast agents, recent innovations have enabled the development of ultra-small SPIONs—such as exceedingly small SPIONs (ES-SPIONs) and single-nanometer iron oxide nanoparticles (SNIOs)—that offer T_1-weighted MRI capabilities, which are favored by radiologists for their superior anatomical clarity. This review highlights the synthesis of monodisperse SPIONs via thermal decomposition and controlled oxidation, as well as their functionalization with zwitterionic dopamine sulfonate (ZDS) ligands, which confer colloidal stability, minimal protein adsorption, and efficient renal clearance. Notably, SNIOs conjugated with collagen-binding peptides (CBPs) enabled rapid, non-invasive detection of liver fibrosis, comparable to mainstream gadolinium-based probes in sensitivity. We further discuss the integration of SPIONs with fluorescent quantum dots to achieve magneto-fluorescent constructs for dual-modal imaging, facilitating simultaneous MR and optical tracking. These advancements collectively position ZDS-coated SPIONs as potential MRI agents with theranostic potential, bridging the gap between fundamental nanoscience and clinical application. This review also addresses ongoing challenges in clinical translation, while outlining a forward-looking vision for SPIONs in personalized, non-invasive diagnostics, biosensing, and targeted therapeutics.

1. Introduction

In recent years, nanomedicine has witnessed transformative advancements through the development of engineered nanoparticles tailored for both therapeutic and diagnostic purposes. Among these, superparamagnetic iron oxide nanoparticles (SPIONs) have emerged as a particularly promising class of nanomaterials due to their unique magnetic response, biocompatibility, and capacity for multifunctional design [1,2]. Their responsiveness to external magnetic fields enables non-invasive manipulation and imaging, making SPIONs highly suitable for a range of biomedical applications, including magnetic resonance imaging (MRI), targeted drug delivery, and hyperthermia treatment [3]. Compared to other magnetic nanoparticles, SPIONs offer a unique combination of high magnetization, minimized toxicity, and tunable surface chemistry, making them excellent candidates for biomedical applications [4,5].

Historically, SPIONs have primarily been utilized as T_2-weighted (T_2-w) MRI contrast agents, offering significant signal darkening and tissue contrast enhancement. However, their potential as positive contrast agents in T_1-weighted (T_1-w) MRI—preferred by radiologists for more precise anatomical resolution—has only recently been realized [6–8]. This shift is primarily due to innovations in nanoparticle synthesis and surface engineering, which have enabled the production of ultra-small SPIONs with a high longitudinal relaxivity-to-transversal relaxivity ratio (r_1/r_2 ratio) and optimized surface coatings that minimize nonspecific interactions [6,9–11]. Our review highlights such developments, mainly focusing on zwitterionic dopamine sulfonate (ZDS)-coated SPIONs, which present a promising alternative to gadolinium-based contrast agents (GBCAs), known for their risks of retention and toxicity in vulnerable patients [12–14], such as nephrogenic systemic fibrosis and gadolinium deposition in the brain [15,16].

One of the primary challenges in SPION development is their synthesis and functionalization, and the effective synthesis of SPIONs is central to their biomedical performance. Aggregation can lead to undesired cellular uptake and clearance by the immune system [17,18]. Therefore, controlling the particle size, crystallinity, and surface characteristics is essential for ensuring reproducibility, minimizing immune clearance, and enhancing physiological stability [19]. Our work has utilized thermal decomposition followed by a post-synthetic oxidation step to yield highly monodisperse iron oxide nanoparticles with tunable

This article is part of a special issue entitled: Nanomedicine published in Biochemical and Biophysical Research Communications.

* Corresponding author.
E-mail address: mgb@mit.edu (M.G. Bawendi).

https://doi.org/10.1016/j.bbrc.2025.152542
Received 16 June 2025; Received in revised form 22 August 2025; Accepted 24 August 2025
Available online 25 August 2025

diameters and robust superparamagnetism [20]. The resulting SPIONs exhibit high colloidal stability and size uniformity, characteristics that are indispensable for translational medicine. Furthermore, by fine-tuning the solvent environment and reaction conditions, we have successfully synthesized exceedingly small SPIONs (ES-SPIONs) and single-nanometer iron oxide nanoparticles (SNIOs), which are tailored for renal clearance, deep tissue imaging, and targeted MRI.

Additionally, surface modification strategies play a crucial role in determining the stability and interactions of SPIONs with biological molecules, and they remain a key determinant of SPION performance in vivo. Conventional coatings, such as dextran, 2,3-dimercaptosuccinic acid (DMSA), and polyethylene-glycol-modified (PEGylated) molecules, often suffer from limitations, including bulky hydrodynamic diameters, aggregation in saline environments, or unintended immune responses [21–24]. In contrast, ZDS, a compact zwitterionic ligand developed in our laboratory, binds firmly to the iron oxide surface via catechol anchoring groups while maintaining a neutral surface charge through its sulfonate and quaternary amine groups. This ligand design confers remarkable stability in high-salt and physiological conditions [9], significantly reducing nonspecific protein adsorption and minimizing cellular uptake [10]. Moreover, ZDS-coated SPIONs (ZDS-SPIONs) retain strong magnetic properties, as evidenced by saturation magnetization values that compare reasonably well with those of bulk maghemite. Notably, the introduction of ZDS incurs minimal size overhead to the inorganic nanoparticle, preserving a compact hydrodynamic diameter that is essential for renal clearance and tissue permeability [25]. For instance, the SNIOs we developed, with a core size as small as 1 nm and a hydrodynamic diameter of 3.1 nm, represent one of the smallest water-soluble SPION formulations to date.

Another critical aspect of SPION research is their comparison to conventional gadolinium-based contrast agents (GBCAs). On the one hand, GBCAs have long been used in MRI, but concerns regarding their risk and accumulation in a small population of patients [26], such as older patients and those with impaired kidney function [27], have spurred interest in alternative imaging agents. On the other hand, SPIONs, due to their sound magnetic properties, can provide excellent contrast enhancement without the concern associated with the heavy metal gadolinium. As a result, the biocompatible and size features of ES-SPIONs and SNIOs can directly translate into practical biomedical advantages. For instance, ES-SPIONs and SNIOs can achieve efficient renal clearance, a previously challenging task for SPION-based agents, making them suitable as a heavy-metal-free alternative for vulnerable patients. Moreover, the compact design enables enhanced tissue penetration, which is crucial for detecting sensitive diseases in dense or fibrotic tissues [28]. Our recent work demonstrated that SNIOs conjugated with collagen-binding peptides (CBP) enabled the rapid and non-invasive detection of liver fibrosis via T_1-w MRI, with comparable efficacy to state-of-the-art GBCA molecular probes [29].

In addition to their use in MRI, SPIONs serve as multifunctional platforms for integrated diagnostics and therapeutic applications. We have developed dual-modal imaging systems by incorporating SPIONs with fluorescent quantum dots into magneto-fluorescent nanostructures, enabling concurrent MR and fluorescence imaging for various targeting applications [30,31]. These nano-constructs allow for real-time tracking of nanoparticles at both macroscopic and cellular levels. Such versatility reflects the growing interest in SPIONs as theranostic agents—capable of combining diagnosis and therapy within a single platform.

In this review, we aim to provide a comprehensive analysis of our recent progress in SPION research, with a particular focus on the synthesis, functionalization, and biomedical applications of ZDS-coated SPIONs. We discuss how tailored nanostructures such as ES-SPIONs and SNIOs advance T_1-w imaging, comparable to traditional GBCAs, and enable novel diagnostic strategies. By bridging chemistry, biology, and clinical needs, this work underscores the potential of SPIONs as next-generation agents in precision nanomedicine.

2. Main text

2.1. Synthesis and compact ligand coating

2.1.1. Thermal Decomposition and post-synthetic oxidation techniques

Our initial investigations emphasized the importance of controlling the size and crystallinity of superparamagnetic iron oxide nanoparticles (SPIONs) through thermal decomposition methods [9]. This approach often involves using high-boiling-point organic solvents that also require high reaction temperatures for the formation of SPION nuclei, leading to precise size control and the production of uniformly sized SPIONs. As shown in Fig. 1a, the primary synthetic procedure in our work employed iron pentacarbonyl or iron oleate precursors in various organic solvents (e.g., 1-tetradecene, 1-hexadecene, 1-octadecene, and dioctyl ether), together with native oleic acid ligands. Moreover, we found that a mixture of multiple organic solvents, rather than a single solvent, can be used to target a specific boiling point and fine-tune SPION nucleation for improved size control. Once the iron precursor decomposes at selected temperatures up to 320 °C and the reaction mixture is incubated for a period of time (usually between 30 min and 2 h), a controlled oxidation step using trimethylamine N-oxide (TMAO) is introduced. This mild oxidation step promotes the formation of maghemite (γ-Fe_2O_3) rather than magnetite (Fe_3O_4), a transition particularly beneficial for T_1-weighted (T_1-w) MRI applications. This is because the full oxidation of Fe^{2+} to Fe^{3+} in maghemite reduces spin-spin interactions that dominate r_2 relaxivity and enhances r_1 via more uniform surface spin dynamics [32]. This contributes to a higher r_1/r_2 ratio, favorable for T_1 contrast. In this process, TMAO converts SPIONs from a wüstite or partially oxidized form into a more stable maghemite phase while preserving monodispersity and strong superparamagnetism at room temperature.

A primary outcome of our synthesis route is the production of uniformly sized SPIONs with inorganic core diameters ranging from 1 to 35 nm (Fig. 1b–g), depending on temperature and solvent choice. These SPIONs usually exhibit narrow size distributions and high crystallinity, as observed by transmission electron microscopy (TEM), X-ray diffraction (XRD), and X-ray Absorption Fine Structure (XAFS) studies. Using this route, SPIONs with any chosen diameter within this range can be synthesized with a precision of 1–2 nm, as illustrated by a series of representative SPIONs in our prior work [20]. It is worth noting that the most miniature version of our SPIONs, the single-nanometer iron oxide (SNIO) nanoparticles [6], can be synthesized by adjusting the solvent composition to a mixture of 1-tetradecene and 1-hexadecene. This allows the reaction temperature and the SPION nucleation temperature to be significantly reduced to 260 °C (compared with typical temperatures of up to 290–320 °C for SPION synthesis when using high-boiling-point solvents such as dioctyl ether or 1-octadecene), where the lower temperature strongly limits Ostwald ripening while preserving superparamagnetic behavior [33,34].

2.1.2. Zwitterionic dopamine sulfonate ligand

Since uniformly sized SPIONs synthesized in organic solvents are generally hydrophobic, they cannot be used directly in aqueous media for biomedical applications. This has prompted the development of various water-soluble ligands. The traditional ligands for SPIONs, such as 2,3-dimercaptosuccinic acid (DMSA), dextran, and polyethylene-glycol-modified (PEGylated) carboxylic acids, suffer from one or a combination of aggregation and large size issues [21–23,35]. As a result, we have designed and synthesized a compact and water-soluble zwitterionic dopamine sulfonate (ZDS) ligand, as shown in Fig. 1a. The catechol moiety in ZDS strongly coordinates with the iron oxide surface [36] of SPIONs, preventing ZDS from being cleaved from the SPION surface and consequently eliminating aggregation concerns. Additionally, the sulfonate and quaternary amine groups in ZDS confer a zwitterionic characteristic, ensuring biocompatibility (Fig. 2a–d) and pH stability [37,38]. Moreover, the ZDS ligand allowed SPIONs to maintain

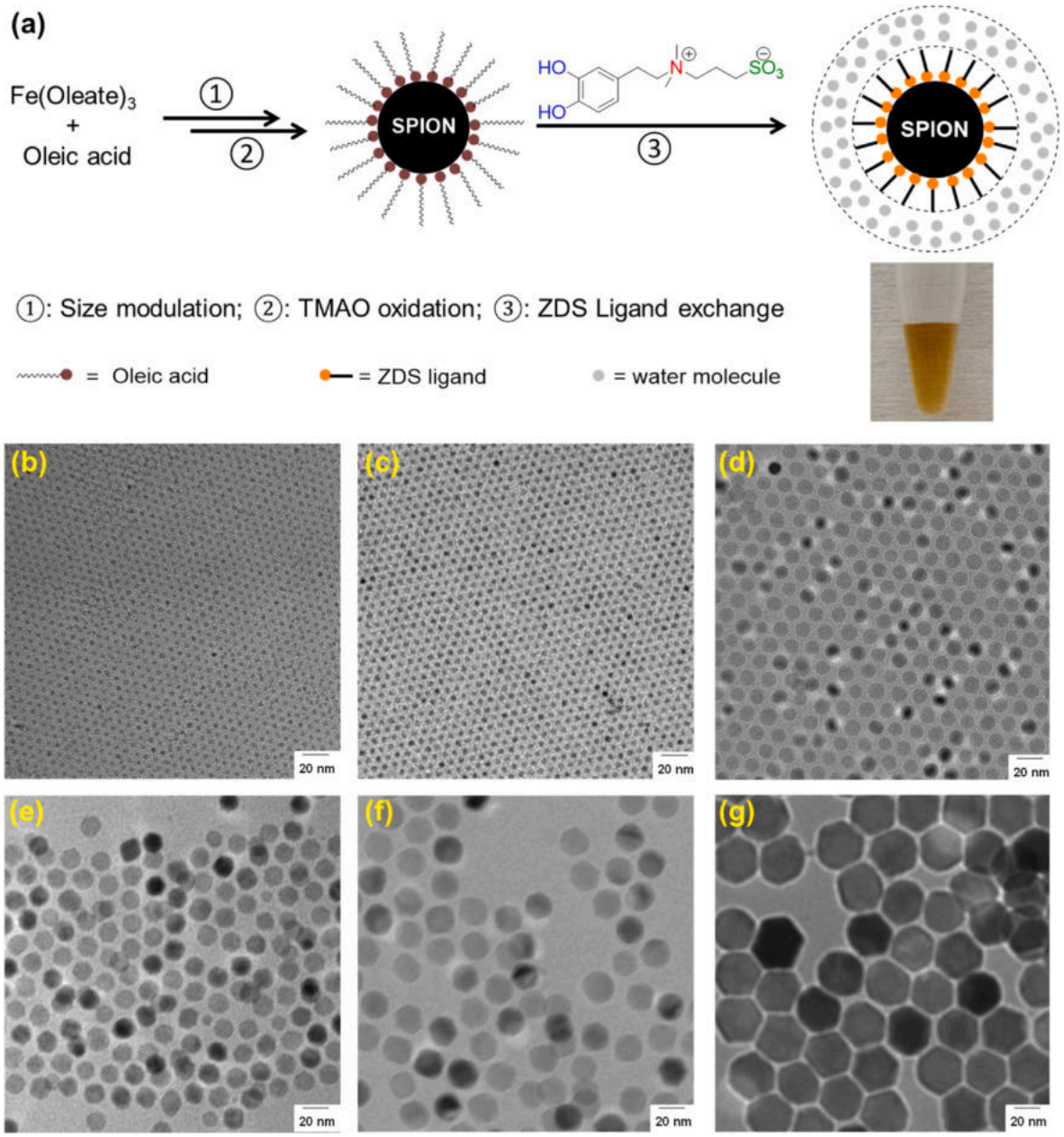

Fig. 1. (a) The synthetic route of zwitterion dopamine sulfonate (ZDS)-coated SPIONs: differently sized maghemite (γ-Fe_2O_3) nanoparticles were produced through the thermal decomposition of an iron oleate precursor and oleic acid under modulated conditions, followed by trimethylamine N-oxide (TMAO) oxidation and ZDS ligand exchange. Inset: Water-soluble ZDS-SPIONs dispersed in phosphate-buffered saline (PBS) 1X. Representative transmission electron microscopy (TEM) images of the as-synthesized monodisperse SPIONs with different inorganic diameters: (b) 3 nm, (c) 5 nm, (d) 12 nm, (e) 16 nm, (f) 20 nm, and (g) 35 nm. Scale bars in (b)–(g): 20 nm. The results were adopted from our prior works [6,10,20] and adapted with permission from the publishers.

their strong superparamagnetism. We have reported that the saturation magnetization (M_s) values for SPIONs before and after the ZDS ligand exchange were almost identical, showing an M_s of 74 emu/g [Fe], which compares reasonably well with the M_s of bulk maghemite mineral (106 emu/g [Fe]) [39]. This robust superparamagnetism of ZDS-coated SPIONs (ZDS-SPIONs) underpins their enhanced MRI contrast in biomedical imaging [40,41].

Further experiments have demonstrated that ZDS-SPIONs formed stable aqueous dispersions over a pH range of 6.0–8.5, as well as in high-salinity environments such as cerebrospinal fluids, cell culture media, or even saturated NaCl solutions [8–10]. In addition to the high stability and hydrophilicity of ZDS-SPIONs, their compact size is another significant advantage over traditional SPIONs, as displayed in Fig. 2e. Through dynamic light scattering (DLS) and size-exclusion chromatography (SEC) measurements, the introduction of the ZDS ligand typically results in an addition of only 2 nm to the hydrodynamic diameter (HD) compared with the inorganic core. Hence, the exceedingly small SPIONs (ES-SPIONs) with 3 nm cores showed an average HD of 4.7 nm, and the average HD of SNIOs with 1 nm cores was merely 3.1 nm, one of the smallest water-soluble SPIONs reported to date [42,43]. These compact sizes improved the ability of ZDS-coated SPIONs to induce positive/hyperintense MR signals and enter intracellular spaces [44,45], as well as enhanced their tissue permeability for various biomedical applications [46].

2.1.3. Colloidal Stability and reduced nonspecific binding

Many established SPION formulations, such as those coated with proteins, carbohydrates, nucleic acids, or lipids, encounter difficulties

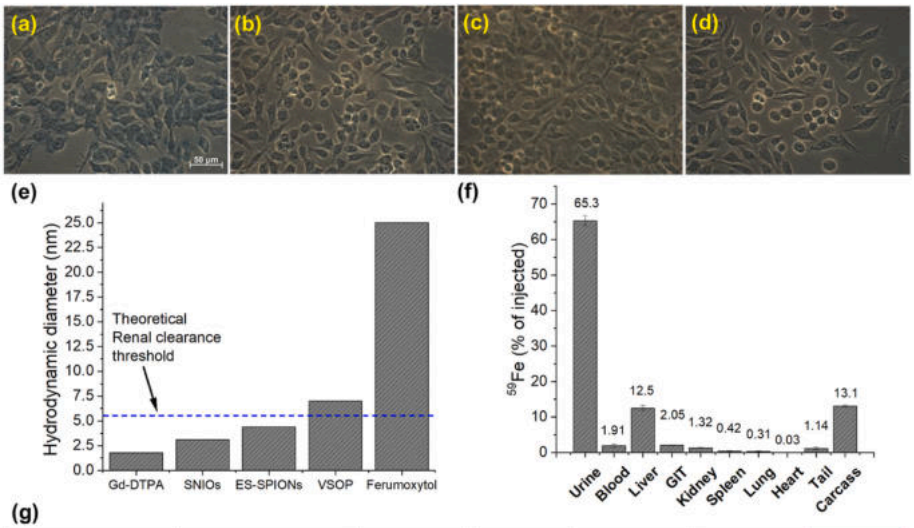

(g)

Field Strength (T)	Species	Core (nm)	HD (nm)	r_1 ($s^{-1}mM^{-1}$)	r_2 ($s^{-1}mM^{-1}$)	r_1/r_2
1.5	Gd-DTPA	Gd^{3+}	1.8	4.8	5.1	0.91
	SNIOs	1	3.1	3.0	3.4	0.91
	ES-SPIONs	3	4.4	5.2	10.5	0.50
	VSOP	4	7	15	32	0.48
	Ferumoxytol	7	20-30	15	89	0.17
7	Gd-DTPA	Gd^{3+}	1.8	4.1	4.3	0.91
	SNIOs	1	3.1	4.9	9.1	0.53
	ES-SPIONs	3	4.4	1.5	17	0.09
	Ferumoxytol	7	20-30	3.1	68	0.05

Fig. 2. (a) Iron uptake studies using HeLa cells and Prussian blue staining, after 24 h of incubation with: a) $FeCl_3$ (2 mg[Fe]/mL), b) control (0 mg[Fe]/mL), c) ZDS-coated SPIONs (2 mg[Fe]/mL), and d) TD/ZDS-coated SPIONs (2 mg[Fe]/mL), showing a minimal uptake of ZDS-SPIONs and TD/ZDS-SPIONs, confirmed by the absence of blue signals in (c)–(d). (e) The hydrodynamic diameters of different MRI contrast agents, where the blue dashed line indicates the theoretical renal clearance threshold of 5.5 nm. Gd-DTPA: gadolinium diethylenetriaminepentaacetic acid (Magnevist®), SNIOs: single-nanometer iron oxide nanoparticles, ES-SPIONs: exceedingly small SPIONs, VSOP: very small iron oxide nanoparticles, and Ferumoxytol: Feraheme®. (f) The percentages of ^{59}Fe-labeled ES-SPIONs that remained in urine, blood, and organs (GIT: gastrointestinal tract) 24 h after their injection. (g) The T_1 and T_2 contrast power, as well as the r_1/r_2 ratio (higher values are preferred for T_1-w MRI), of the five contrast agents. The results were adopted from our prior works [6,8,10] and adapted with permission from the publishers. (For interpretation of the references to colour in this figure legend, the reader is referred to the Web version of this article.)

with nonspecific binding and salt-driven aggregation [47,48]. Negatively charged SPIONs, including those coated with pure silica shells or multidentate carboxylic molecules, also exhibit nonspecific binding to positively charged species in biological media [49,50]. In contrast, size-exclusion chromatography (SEC) and high-performance liquid chromatography (HPLC) stability tests confirmed that ZDS-SPIONs largely retained their original HD when exposed to fetal bovine serum in vitro and mouse blood in vivo, resulting in minimal shifts in elution time, as characterized by SEC and HPLC. This outcome is attributed to the near-neutral surface charge provided by ZDS ligands, diminishing electrostatic interactions. Using radioisotope-labeled (^{59}Fe) ZDS-SPIONs in recent studies, it was demonstrated that ZDS-SPIONs remained stable in circulation and exhibited minimal sequestration in the liver and spleen, unlike larger or electrostatically charged particles, which are generally affected.

2.1.4. *Biomedical functionality*

A binary coating design consisting of ZDS and a secondary ligand can be applied to SPIONs to endow them with bio-conjugatable capability. Here, the ZDS ligand provides water solubility, while the secondary ligand offers functionality. We have synthesized a short-chain catechol-thiol secondary ligand (TD ligand), and other research groups have reported the use of glutathione, cysteine, lysine, and tris(hydroxymethyl) aminomethane [51] as the secondary ligands for various applications. A proof-of-concept sensing experiment was achieved by conjugating an Alexa Fluor 488 maleimide dye (Dye488) and a streptavidin maleimide (SA) moiety with SPIONs coated by 85 % ZDS ligand and 15 % TD ligand (mol%). The resulting nano-construct can specifically label biotin molecules and induce a more than 10-fold increase in fluorescence compared to the biotin-free environment. This demonstrates that the ZDS/TD-coated and other types of coated SPIONs [52,53] developed by us have the potential to be conjugated to the maleimide group from peptides, aptamers, antibodies, or proteins of interest [54,55], rendering them suitable for in vitro and in vivo targeted imaging and sensing applications.

2.2. *MRI contrast properties and applications*

2.2.1. *T_1-and T_2 MRI contrast power*

SPIONs traditionally serve as T_2 contrast agents, where larger iron oxide cores ($\geq$6 nm) produce strong negative/hypointense contrast due to their high transversal relaxivity (r_2), leading to a darkening effect in MRI. T_1-weighted MRI contrast from SPIONs arises through spin-lattice relaxation, where unpaired 3d electrons in Fe^{3+} ions interact magnetically with nearby water protons. These dipole-dipole interactions and fluctuating local magnetic fields facilitate energy transfer that shortens the T_1 relaxation time [56]. In ultrasmall SPIONs with cores smaller than ~5 nm, rapid magnetic moment fluctuations, enhanced by surface spin disorder and superparamagnetism, promote high longitudinal relaxivity (r_1), enabling effective T_1 contrast enhancement. Notably, our recent

studies on SPIONs have shown that iron oxide cores below 3 nm can exhibit a reduced r_2 while maintaining a high r_1, resulting in positive/hyperintense contrast and making them preferred for T_1-weighted (T_1-w) MRI. For example, as shown in Fig. 2g, ZDS-coated exceedingly small SPIONs (ES-SPIONs) with a 3-nm core and a 4.7-nm hydrodynamic diameter (HD) demonstrated an r_1 of 5.2 s^{-1} mM^{-1} and an r_2 of 10.5 s^{-1} mM^{-1}, achieving an attractive r_2/r_1 ratio of 2.0, comparable to heavy-metal gadolinium-based contrast agents (GBCAs). The single-nanometer iron oxide nanoparticles (SNIOs) with even smaller cores (1 nm) produced a nearly ideal r_2/r_1 ratio close to 1, effectively mimicking the T_1 contrast power of paramagnetic GBCAs while avoiding toxicity concerns for older patients and patients with impaired kidney functions [15,16,26,27,57,58]. More recently, trace amounts of gadolinium have been observed in organs after GBCA exposure, even for patients with normal renal function [12].

2.2.2. *Renal Clearance and T_1-w MR imaging*

One of the primary challenges in conventional SPIONs for MRI applications is the lack of efficient and rapid renal clearance from the body. Previous SPION formulations with large hydrodynamic diameters generally accumulate in the liver and spleen [59,60], limiting their use in repeated MR imaging and diagnosis and potentially leading to iron overdose. In contrast to conventional SPIONs, ES-SPIONs with a 4.7-nm HD fall below the renal clearance cutoff (i.e., the glomerular filtering threshold) of ~5.5 nm, as demonstrated in Fig. 3a–j [61]. Therefore, 24 h after intravenous injection, ES-SPIONs demonstrated renal clearance ratios of 65 %, as quantified by ^{59}Fe radioisotope labeling experiments (Fig. 2f), with most of the nanoparticles excreted through the renal route within 4 h. This number compares reasonably well with the renal clearance ratios of GBCAs, which are approximately 80–90 % [13,14]. We further showcased the preclinical potential of ES-SPIONs using T_1-w MR angiography (MRA), whose in vivo half-life in mouse blood was determined to be 19 min. The efficient renal clearance of ES-SPIONs was again confirmed by the increasing hyperintense MR signal in the mouse bladder within several minutes after the contrast agent injection. Moreover, ES-SPIONs enabled a 5-fold relative signal enhancement in mouse blood, with essentially no significant signal enhancement in muscle. This considerable signal-to-noise ratio allowed us to perform a three-dimensional reconstruction of mouse blood vessels and even capillaries, as shown in Fig. 3k–o.

2.2.3. *Tissue Permeation and targeted MR imaging*

Our single-nanometer iron oxide nanoparticles (SNIOs) with an HD of 3.1 nm have demonstrated potent diffusion in dense biological tissues, as illustrated by the successful infusion and spread of SNIOs into the rodent brain parenchyma. Moreover, through in vivo cerebrospinal fluid

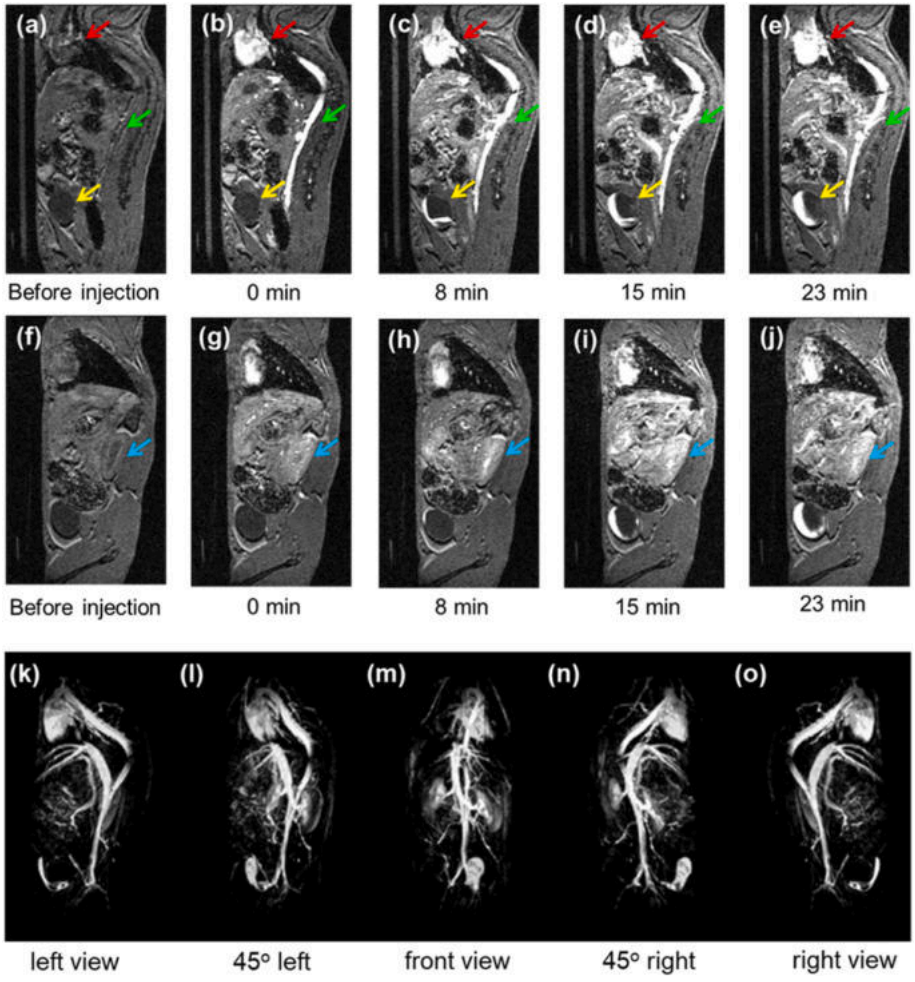

Fig. 3. T_1-w MR images of a representative mouse injected with exceedingly small ZDS-coated SPIONs (ES-SPIONs) at 7 T. (a)–(e) a sagittal slice showing the heart (red arrow), the vena cava (green arrow), and the bladder (yellow arrow), and (f)–(j) another sagittal slice showing the kidney (blue arrow). The time points listed below each image indicate the time post-ES-SPION injection, and the positive/hyperintense MR signals result from ES-SPIONs, confirming their timely renal clearance. (k)–(o) Five different perspectives of the three-dimensional T_1-w magnetic resonance angiography (MRA) at 4 min post-ES-SPION injection. Clear positive contrasts of the heart, kidneys, bladder, and blood vessels were observed. The results were adopted from our prior work [6] and adapted with permission from the publisher. (For interpretation of the references to colour in this figure legend, the reader is referred to the Web version of this article.)

injections and T_1-w MR imaging, SNIOs were distributed across nearly the entire rat brain, resulting in brain-wide hyperintense MR signals (Fig. 4a) and displaying their potential for neurobiological imaging across the brain. Furthermore, we investigated the use of SNIOs in crossing the blood-brain barrier (BBB). The ultrasound-mediated BBB disruption (Fig. 4b), a clinically approved technique, allows the intravenously injected SNIOs to exit the vasculature into targeted cerebral areas, producing widespread T_1 contrast changes in the group of four rats' right hemispheres treated by ultrasound, while the rats' left hemispheres without ultrasound showed no contrast change (Fig. 4c). The observed MR signal changes induced by SNIOs and their delivery efficiency were comparable to those of gadolinium diethylenetriaminepentaacetic acid (Gd-DTPA, Magnevist®). While GBCA remains the mainstream agent for MRI-based brain imaging, SNIOs may offer a heavy-metal-free and effective alternative with higher molecular efficiency (i.e., r_1 per molecule/nanoparticle) in T_1 contrast enhancement.

More recently, we have extended the application of SNIOs by integrating type I collagen-binding peptides (CBP) onto nanoparticle surfaces (Fig. 5a), creating a highly sensitive MRI contrast agent for fast and non-invasive detection of liver fibrosis [62]. The functionalized SNIO-CBP exhibited nearly 7-fold higher relaxivity compared with a molecular gadolinium-based collagen-binding contrast agent (CM-101) on a per CBP basis at 4.7 T. Moreover, in contrast to conventional SPION formulations, SNIO-CBP exhibited rapid elimination from the mouse bloodstream ($t_{1/2} = 5.7$ min) and efficient renal clearance. While the T_1 contrast enhancement in healthy mice was low and transient because SNIO-CBP did not target healthy hepatic cells, SNIO-CBP in T_1-w MRI was able to swiftly detect hepatotoxin-induced liver fibrosis within 15 min using a carbon tetrachloride-induced mouse liver injury model, showing a 2.5 times higher dose efficacy than that of gadolinium-based CM-101 (Fig. 5b). The SNIO-CBP development offers a high relaxivity and gadolinium-free MRI sensor for diagnosing chronic liver diseases using the radiologist-preferred T_1-w MRI compared with previous T_2-w MRI-based SPION probes for liver fibrosis [63,64]. This further marks a significant step forward in the potential clinical translation of SNIOs.

2.2.4. MR and fluorescent dual-modal imaging

Dual-modal imaging has emerged as a potentially transformative technique, offering synergistic capabilities for real-time visualization and targeted manipulation in biomedical applications [66,67]. For this reason, we initially developed a synthesis method for ~500 nm monodisperse silica microspheres embedded with SPIONs and fluorescent quantum dots (QDs) [68]. These microspheres demonstrated uniform incorporation of QDs and SPIONS within the silica shell, maintaining structural integrity and enabling magnetic manipulation alongside real-time fluorescence imaging. On average, up to 13,000 SPIONs and 4600 QDs were successfully integrated per microsphere. Moreover, external magnetic fields enabled precise control over microsphere positioning, paving the way for targeted drug delivery and cellular studies via multimodal imaging using both magnetic resonance and fluorescence.

To reduce the size of the bifunctional microspheres, we subsequently constructed core-shell supernanoparticles (CS-SPs, Fig. 6a and b) through the co-assembly of SPIONs and QDs [65,69]. The ~100 nm superparamagnetic and fluorescent CS-SPs showed high colloidal stability, efficient PEGylation for biocompatibility, magnetic separation potential (Fig. 6c), and exceptional dual-modal imaging functionality. We also demonstrated their in vivo applications, including successful magnetic manipulation within live cells and dual-modal multi-photon and MR imaging in mouse brain tumor models, revealing substantial structural information of the tumor site and imaging clarity (Fig. 6d and e). These innovations underscore the potential of SPION-based dual--functional nano-assemblies for advanced imaging, diagnostics, and therapeutic delivery [70,71], laying a robust foundation for continued exploration in nanomedicine.

3. Challenges and future directions

Even though iron oxide is generally a type of material with minimized toxicity and excellent stability, the biocompatibility and toxicity considerations for SPIONs remain a central topic in their clinical applications. It is worth noting that, while iron oxide cores have the

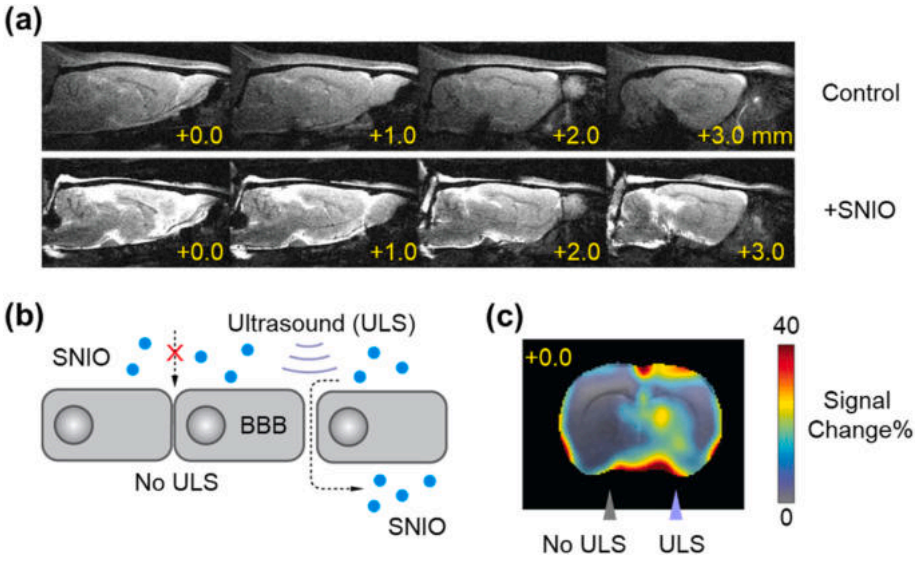

Fig. 4. (a) T_1-w MRI scans of a representative rat brain indicating the contrast change induced by single-nanometer iron oxide nanoparticles (SNIOs). Top and bottom rows are the brain sagittal slices before and after the SNIO injection through the intracisternal route. Yellow labels denote the mediolateral position in mm from the rat brain's midline. (b) Transcranial ultrasound (ULS) can disrupt junctions between cells that form the blood-brain barrier, allowing intravenously injected SNIOs to successfully enter the brain tissue. A transducer operating at a driving frequency of 500 kHz was deployed with the following ultrasound parameters: 0.2 V input amplitude, 5000 burst count, and a 1-s burst repetition rate. (c) Average percentage signal changes observed before and after the intravenous SNIO injection in a group of four rats. In the shown coronal slide (anteroposterior position = 0.0 mm from the bregma), no ULS was applied to the left hemisphere, while ULS was applied to the right hemisphere. The results were adopted from our prior work [8] and adapted with permission from the publisher. (For interpretation of the references to colour in this figure legend, the reader is referred to the Web version of this article.)

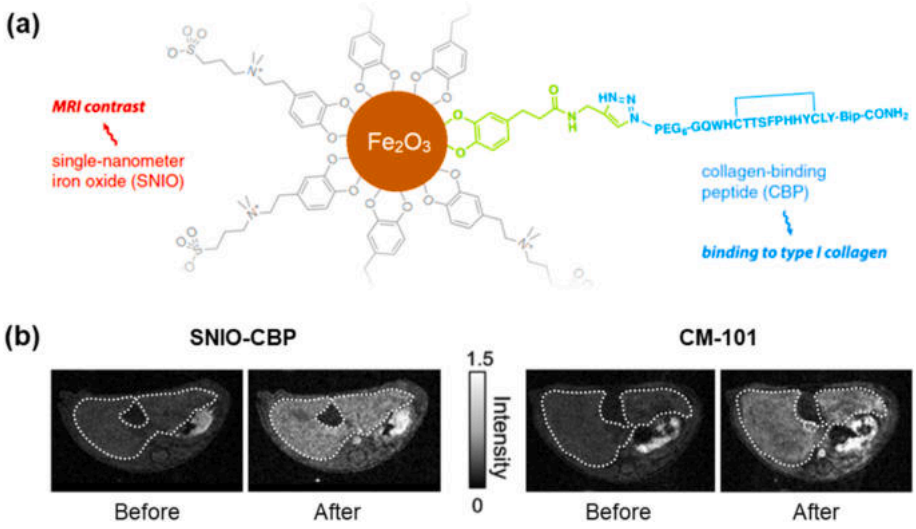

Fig. 5. (a) Schematic illustration of the construction of SNIOs functionalized with a type I collagen-binding peptide (SNIO-CBP). Two types of ligands are present on the nanoparticle surface: zwitterionic ligands offer stability and solubility, peptide-conjugated ligands allow for targeting. (b) T_1-w MRI of two mice with CCl_4-induced liver fibrosis. Left: Before and 13 min after the injection of SNIO-CBP (2 nmol/g CBP); Right: Before and 13 min after the injection of a gadolinium-based collagen-binding contrast agent (CM-101, 5 nmol/g CBP). The results were adopted from our prior work [62] and adapted with permission from the publisher.

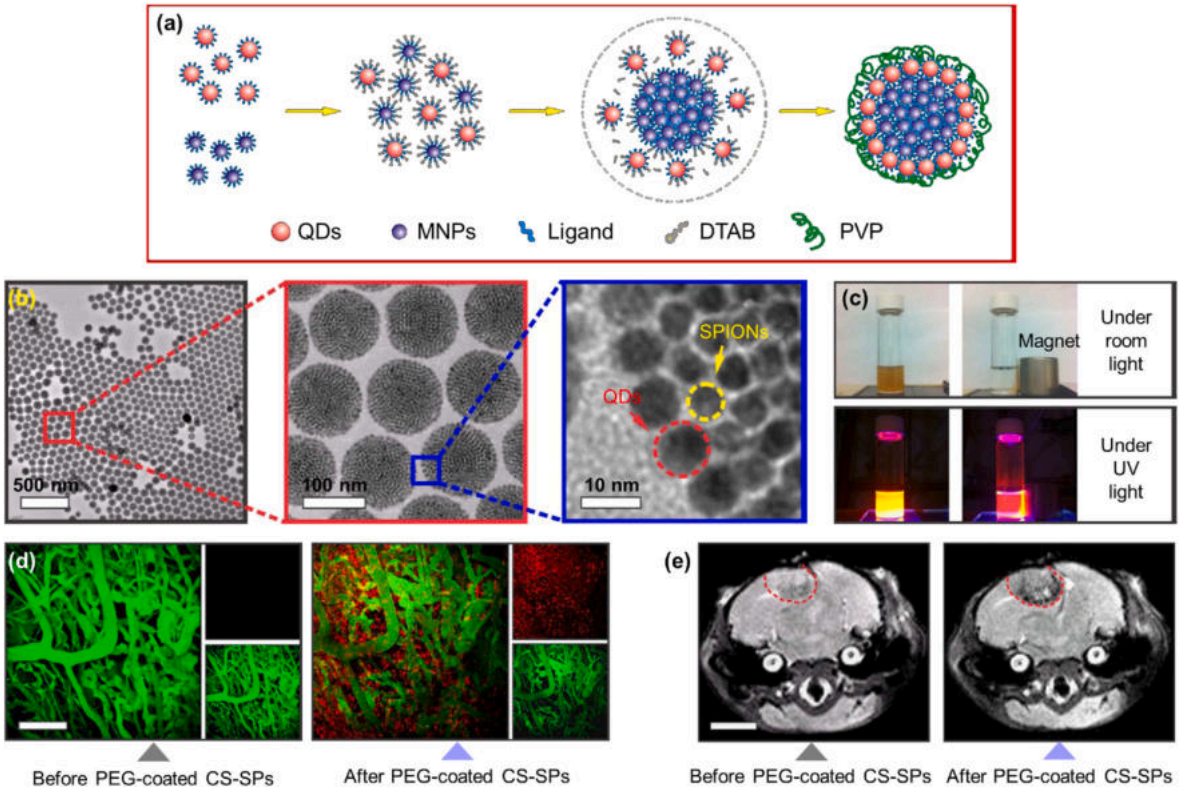

Fig. 6. (a) Schematic of the formation of the core-shell supernanoparticles (CS-SPs). DTAB: dodecyltrimethylammonium bromide; PVP: poly(vinylpyrrolidone). (b) TEM images of CS-SPs via the co-assembly of SPIONs and fluorescent quantum dots at different magnifications. (c) Photographs demonstrating the magnetic separation of CS-SPs using a magnet under the room light (top) and ultraviolet light (bottom). (d) Using a C3H mouse model with brain metastasis of a murine mammary carcinoma and a cranial window, intravital multiphoton microscopy through the cranial window was performed before (left) and 24 h after (right) the intravenous injection of mPEG-coated CS-SPs containing red fluorescent quantum dots and SPIONs. Green emission signals resulted from a blood vessel tracer (fluorescein isothiocyanate–dextran), while red emission signals originated from PEG-coated CS-SPs. Images from individual red and green channels are shown in the insets. Scale bar: 150 μm. Scale bar: 3 mm. (e) Using the same mouse model, T_2-w MRI scans were carried out before (left) and 24 h after (right) the intravenous injection of mPEG-coated CS-SPs, where the tumor site was visualized and denoted by the red dashed lines. Scale bar: 3 mm. The results were adopted from our prior work [65] and adapted with permission from the publisher. (For interpretation of the references to colour in this figure legend, the reader is referred to the Web version of this article.)

potential to generate reactive oxygen species (ROS) under certain conditions, toxicity can be effectively mitigated through the use of robust surface coatings [72], such as the ZDS ligand, which prevent oxidative stress and cellular damage in biological environments. Despite the growing interest in ZDS-SPIONs for biomedical imaging and theranostic applications, their long-term biocompatibility and toxicity are important concerns that encourage a comprehensive investigation. While our in vitro results using HeLa cells have demonstrated minimal nonspecific iron uptake (Fig. 2a–d), implying low cytotoxicity and favorable interaction with cellular environments [10], in vitro models often do not fully capture the complexity of in vivo physiological responses. Similarly, our in vivo studies in rodent models did not reveal overt toxic effects, nor did we observe significant weight loss or distress in mice and rats following administration of ZDS-SPIONs during biodistribution, imaging, and targeting studies [6,8,62]. Nevertheless, these findings must be interpreted cautiously, as long-term outcomes, particularly those involving repeated or high-dose administration, have yet to be systematically evaluated.

A major next step in the clinical translation of ZDS-SPIONs is a robust assessment of their pharmacokinetics, biodistribution, and clearance in larger animal models, such as rabbits or non-human primates. These models provide physiologically relevant data that more closely mimic human metabolic and immunological processes, helping identify potential immunogenic responses, off-target effects, and organ accumulation patterns that may not manifest in rodents [17,73]. In parallel, a thorough histopathological evaluation of organs—particularly the liver, spleen, kidneys, and brain—following chronic exposure to ZDS-SPIONs will be essential to rule out subclinical toxicity, iron overload, or nanoparticle aggregation within the mononuclear phagocyte system.

Furthermore, an important challenge lies in understanding the degradation and long-term fate of SPIONs within biological environments. Unlike small molecules, nanoparticle degradation and clearance involve complex interactions with biological fluids, proteins, and cells [74,75]. It is not yet clear whether surface coatings such as ZDS undergo enzymatic cleavage or structural alteration in vivo, which could alter the SPIONs' colloidal stability or magnetic properties over time. These transformations may also influence their MRI relaxivity and imaging performance, particularly if surface charge or hydrodynamic diameter changes during circulation. As a result, the reliable clinical deployment of ZDS-SPIONs demands a deeper mechanistic understanding of their in vivo transformations to ensure consistent diagnostic performance and safety.

4. Conclusion

In this review, we have traced our progress in the development of superparamagnetic iron oxide nanoparticles (SPIONs) optimized for T_1-w MRI, particularly highlighting our contributions to their synthesis, surface modification, and biomedical applications. Our work has demonstrated that thermal decomposition coupled with controlled oxidation yields highly monodisperse SPIONs with tunable sizes and robust superparamagnetism - key features for reliable performance in nanomedicine. Zwitterionic dopamine sulfonate (ZDS) ligands have proven vital in achieving aqueous stability, biocompatibility, and minimal nonspecific binding, setting a new benchmark for SPION surface functionalization. A major accomplishment is the successful design and realization of exceedingly small SPIONs (ES-SPIONs) and single-nanometer iron oxide nanoparticles (SNIOs) with effective T_1-weighted MRI contrast, matching that of gadolinium-based contrast agents (GBCAs) while offering a safer profile, particularly for patients with kidney impairments. Furthermore, by achieving renal-clearable SPIONs and integrating collagen-binding peptides, we introduced a non-invasive imaging strategy for detecting liver fibrosis, with potential for pre-clinical diagnostics.

The expansion of SPION functionality into dual-modal imaging with magneto-fluorescent constructs underscores their vast potential in real-time diagnostics, intracellular tracking, and theranostics. As we move forward, challenges such as long-term toxicity studies, manufacturing scalability, and regulatory validation must be addressed. Nonetheless, our findings illuminate a promising path toward clinical translation. Looking ahead, the combination of SPION technology with innovative diagnostics heralds a future where personalized, non-invasive, and precise medical interventions become standard. SPIONs, once used solely as contrast enhancers, now stand poised to redefine targeted molecular imaging and nanotherapeutics. Continued interdisciplinary efforts will undoubtedly unlock their full potential, marking an exciting era in the field of nanomedicine.

CRediT authorship contribution statement

He Wei: Writing – review & editing, Writing – original draft, Visualization, Methodology, Formal analysis, Data curation. **Moungi G. Bawendi:** Writing – review & editing, Writing – original draft, Supervision, Resources, Project administration, Methodology, Funding acquisition, Formal analysis, Conceptualization.

Declaration of competing interest

The authors declare the following financial interests/personal relationships which may be considered as potential competing interests: Moungi G. Bawendi has patent #Compact nanoparticles for biological applications (US9078920B2) issued to N/A. He Wei has patent #Compact nanoparticles for biological applications (US9078920B2) issued to N/A. Moungi G. Bawendi has patent #Nanoparticles for magnetic resonance imaging applications (US10758633B2) issued to N/A. He Wei has patent #Nanoparticles for magnetic resonance imaging applications (US10758633B2) issued to N/A. Moungi G. Bawendi has patent #Nanoparticles for magnetic particle imaging applications (US20160136307A1) pending to N/A. He Wei has patent #Nanoparticles for magnetic particle imaging applications (US20160136307A1) pending to N/A. If there are other authors, they declare that they have no known competing financial interests or personal relationships that could have appeared to influence the work reported in this paper.

References

[1] M.I. Anik, M.K. Hossain, I. Hossain, A.M.U.B. Mahfuz, M.T. Rahman, I. Ahmed, Recent progress of magnetic nanoparticles in biomedical applications: a review, Nano Select 2 (6) (2021) 1146–1186, https://doi.org/10.1002/nano.202000162.
[2] B. Lee, Y. Lee, N. Lee, D. Kim, T. Hyeon, Design of oxide nanoparticles for biomedical applications, Nat. Rev. Mater. (2025) 1–16, https://doi.org/10.1038/s41578-024-00767-x.
[3] M.G. Montiel Schneider, M.J. Martín, J. Otarola, E. Vakarelska, V. Simeonov, V. Lassalle, M. Nedyalkova, Biomedical applications of iron oxide nanoparticles: current insights progress and perspectives, Pharmaceutics 14 (1) (2022) 204, https://doi.org/10.3390/pharmaceutics14010204.
[4] H.-V. Tran, N.M. Ngo, R. Medhi, P. Srinoi, T. Liu, S. Rittikulsittichai, T.R. Lee, Multifunctional iron oxide magnetic nanoparticles for biomedical applications: a review, Materials 15 (2) (2022) 503, https://doi.org/10.3390/ma15020503.
[5] Z. Ma, J. Mohapatra, K. Wei, J.P. Liu, S. Sun, Magnetic nanoparticles: synthesis, anisotropy, and applications, Chem Rev 1c00860 (2021), https://doi.org/10.1021/acs.chemrev.1c00860.
[6] H. Wei, O.T. Bruns, M.G. Kaul, E.C. Hansen, M. Barch, A. Wiśniowska, O. Chen, Y. Chen, N. Li, S. Okada, J.M. Cordero, M. Heine, C.T. Farrar, D.M. Montana, G. Adam, H. Ittrich, A. Jasanoff, P. Nielsen, M.G. Bawendi, Exceedingly small iron oxide nanoparticles as positive MRI contrast agents, Proc. Natl. Acad. Sci. USA 114 (9) (2017) 2325–2330, https://doi.org/10.1073/pnas.1620145114.
[7] T.H. Shin, P.K. Kim, S. Kang, J. Cheong, S. Kim, Y. Lim, W. Shin, J.Y. Jung, J. D. Lah, B.W. Choi, J. Cheon, High-resolution T1 MRI via renally clearable dextran nanoparticles with an iron oxide shell, Nat. Biomed. Eng. 5 (3) (2021) 252–263, https://doi.org/10.1038/s41551-021-00687-z.
[8] H. Wei, A. Wiśniowska, J. Fan, P. Harvey, Y. Li, V. Wu, E.C. Hansen, J. Zhang, M. G. Kaul, A.M. Frey, G. Adam, A.I. Frenkel, M.G. Bawendi, A. Jasanoff, Single-nanometer iron oxide nanoparticles as tissue-permeable MRI contrast agents, Proc. Natl. Acad. Sci. USA 118 (42) (2021) e2102340118, https://doi.org/10.1073/pnas.2102340118.

[9] H. Wei, N. Insin, J. Lee, H.-S. Han, J.M. Cordero, W. Liu, M.G. Bawendi, Compact zwitterion-coated iron oxide nanoparticles for biological applications, Nano Lett. 12 (1) (2012) 22–25, https://doi.org/10.1021/nl202721q.
[10] H. Wei, O.T. Bruns, O. Chen, M.G. Bawendi, Compact zwitterion-coated iron oxide nanoparticles for *In vitro* and *In vivo* imaging, Integr. Biol. 5 (1) (2013) 108–114, https://doi.org/10.1039/c2ib20142a.
[11] M. Suh, J.Y. Park, G.B. Ko, J.Y. Kim, D.W. Hwang, L. Rees, G.E. Conway, S.H. Doak, H. Kang, N. Lee, T. Hyeon, Y.-S. Lee, D.S. Lee, Optimization of micelle-encapsulated extremely small sized iron oxide nanoparticles as a T1 contrast imaging agent: biodistribution and safety profile, J. Nanobiotechnol. 22 (1) (2024) 419, https://doi.org/10.1186/s12951-024-02699-8.
[12] J.C. Weinreb, R.A. Rodby, J. Yee, C.L. Wang, D. Fine, R.J. McDonald, M. A. Perazella, J.R. Dillman, M.S. Davenport, Use of intravenous gadolinium-based contrast media in patients with kidney disease: consensus statements from the American college of radiology and the national kidney foundation, Radiology 298 (1) (2021) 28–35, https://doi.org/10.1148/radiol.2020202903.
[13] J. Davies, P. Siebenhandl-Wolff, F. Tranquart, P. Jones, P. Evans, Gadolinium: Pharmacokinetics and toxicity in humans and laboratory animals following contrast agent administration, Arch. Toxicol. 96 (2) (2022) 403–429, https://doi.org/10.1007/s00204-021-03189-8.
[14] B.Y.C. Cheong, J.M. Wilson, O.A. Preventza, R. Muthupillai, Gadolinium-based contrast agents: updates and answers to typical questions regarding gadolinium use, Tex. Heart Inst. J. 49 (3) (2022) e217680, https://doi.org/10.14503/THIJ-21-7680.
[15] J. Perez-Rodriguez, S. Lai, B.D. Ehst, D.M. Fine, D.A. Bluemke, Nephrogenic systemic fibrosis: incidence, associations, and effect of risk factor assessment-report of 33 cases, Radiology 250 (2) (2009) 371–377, https://doi.org/10.1148/radiol.2502080498.
[16] T. Kanda, M. Osawa, H. Oba, K. Toyoda, J. Kotoku, T. Haruyama, K. Takeshita, S. Furui, High signal intensity in dentate nucleus on unenhanced T1-Weighted MR images: association with linear versus macrocyclic gadolinium chelate administration, Radiology 275 (3) (2015) 803–809, https://doi.org/10.1148/radiol.14140364.
[17] J. Nowak-Jary, B. Machnicka, Pharmacokinetics of magnetic iron oxide nanoparticles for medical applications, J. Nanobiotechnol. 20 (1) (2022) 305, https://doi.org/10.1186/s12951-022-01510-w.
[18] Y. Xia, J. Zhang, G. Liu, J. Wolfram, Immunogenicity of extracellular vesicles, Adv. Mater. 36 (33) (2024) 2403199, https://doi.org/10.1002/adma.202403199.
[19] P.S. Chary, S. Shaikh, V. Bhavana, N. Rajana, R. Vasave, N.K. Mehra, Emerging role of nanocrystals in pharmaceutical applications: a review of regulatory aspects and drug development process, Appl. Mater. Today 40 (2024) 102334, https://doi.org/10.1016/j.apmt.2024.102334.
[20] H. Wei, Synthesis and Development of Hydrophilic Iron Oxide Nanoparticles for Biomedical Applications, Massachusetts Institute of Technology, Cambridge, MA 02139, USA, 2014. Doctoral Thesis.
[21] M. Salehipour, S. Rezaei, J. Mosafer, Z. Pakdin-Parizi, A. Motaharian, M. Mogharabi-Manzari, Recent advances in polymer-coated iron oxide nanoparticles as magnetic resonance imaging contrast agents, J Nanopart Res 23 (2) (2021) 48, https://doi.org/10.1007/s11051-021-05156-x.
[22] M. Gupta, M. Sharma, Study of dynamical behavior of magnetic nanoparticles suspension in biological fluids, Colloid and Interface Science Communications 37 (2020) 100299, https://doi.org/10.1016/j.colcom.2020.100299.
[23] M.K. Dinker, M.-M. Li, Y. Liu, M. Zuo, L. Ding, J. Kou, L.-B. Sun, What matters to fabrication of type II porous liquids: a case study on metallocages and bulky ionic liquid? Small 20 (43) (2024) 2403174 https://doi.org/10.1002/smll.202403174.
[24] C. Bento, M. Katz, M.M.M. Santos, C.A.M. Afonso, Striving for uniformity: a review on advances and challenges to achieve uniform polyethylene glycol, Org. Process Res. Dev. 28 (4) (2024) 860–890, https://doi.org/10.1021/acs.oprd.3c00428.
[25] B. Lu, J. Wang, A. Jan Hendriks, T.M. Nolte, Clearance of nanoparticles from blood: effects of hydrodynamic size and surface coatings, Environ. Sci. Nano 11 (1) (2024) 406–417, https://doi.org/10.1039/D3EN00812F.
[26] R.J. McDonald, J.S. McDonald, D.F. Kallmes, M.E. Jentoft, D.L. Murray, K. R. Thielen, E.E. Williamson, L.J. Eckel, Intracranial gadolinium deposition after contrast-enhanced MR imaging, Radiology 275 (3) (2015) 772–782, https://doi.org/10.1148/radiol.15150025.
[27] E. Kanal, M.F. Tweedle, Residual or retained gadolinium: practical implications for radiologists and our patients, Radiology 275 (3) (2015) 630–634, https://doi.org/10.1148/radiol.2015150805.
[28] S.L. Gaytan, E. Beaven, S.S. Gadad, M. Nurunnabi, Progress and prospect of nanotechnology for cardiac fibrosis treatment, Interdisciplinary Medicine 1 (4) (2023) e20230018, https://doi.org/10.1002/INMD.20230018.
[29] C.T. Farrar, E.M. Gale, R. Kennan, I. Ramsay, R. Masia, G. Arora, K. Looby, L. Wei, J. Kalpathy-Cramer, M.M. Bunzel, C. Zhang, Y. Zhu, T.E. Akiyama, M. Klimas, S. Pinto, H. Diyabalanage, K.K. Tanabe, V. Humblet, B.C. Fuchs, P. Caravan, CM-101: type I collagen–targeted MR imaging probe for detection of liver fibrosis, Radiology 287 (2) (2018) 581–589, https://doi.org/10.1148/radiol.2017170595.
[30] A.M. Lankoff, M. Czerwińska, M. Kruszewski, Advances in nanotheranostic systems for concurrent cancer imaging and therapy: an overview of the last 5 years, Molecules 29 (24) (2024) 5985, https://doi.org/10.3390/molecules29245985.
[31] Z. Wei, Y. Wu, Y. Zhao, L. Mi, J. Wang, J. Wang, J. Zhao, L. Wang, A. Liu, Y. Li, W. Wei, Y. Zhang, S. Liu, Multifunctional nanoprobe for cancer cell targeting and simultaneous fluorescence/magnetic resonance imaging, Anal. Chim. Acta 938 (2016) 156–164, https://doi.org/10.1016/j.aca.2016.07.037.
[32] S. Chen, L. An, S. Yang, Low-molecular-weight Fe(III) complexes for MRI contrast agents, Molecules 27 (14) (2022) 4573, https://doi.org/10.3390/molecules27144573.
[33] T. van Westen, R.D. Groot, Effect of temperature cycling on ostwald ripening, Cryst. Growth Des. 18 (9) (2018) 4952–4962, https://doi.org/10.1021/acs.cgd.8b00267.
[34] G. Madras, B.J. McCoy, Temperature effects on the transition from nucleation and growth to ostwald ripening, Chem. Eng. Sci. 59 (13) (2004) 2753–2765, https://doi.org/10.1016/j.ces.2004.03.022.
[35] D. Radziuk, A. Skirtach, G. Sukhorukov, D. Shchukin, H. Mohwald, Stabilization of silver nanoparticles by polyelectrolytes and Poly(Ethylene glycol), Macromol. Rapid Commun. 28 (7) (2007) 848–855, https://doi.org/10.1002/marc.200600895.
[36] F. Schwarz, S. Pomp, P. Seidel, X. Li, J. Paier, M. Sterrer, Hydrogen-bond-stabilized high density catechol monolayer on magnetite Fe3O4(111), Surf. Sci. 719 (2022) 122027, https://doi.org/10.1016/j.susc.2022.122027.
[37] K. Qu, Z. Yuan, Y. Wang, Z. Song, X. Gong, Y. Zhao, Q. Mu, Q. Zhan, W. Xu, L. Wang, Structures, properties, and applications of zwitterionic polymers, ChemPhysMater 1 (4) (2022) 294–309, https://doi.org/10.1016/j.chphma.2022.04.003.
[38] Y.K. Jung, E. Shin, B.-S. Kim, Cell nucleus-targeting zwitterionic carbon dots, Sci. Rep. 5 (1) (2015) 18807, https://doi.org/10.1038/srep18807.
[39] C.J. Serna, M.P. Morales, Maghemite (γ-Fe2O3): a versatile magnetic colloidal material, in: E. Matijević, M. Borkovec (Eds.), Surface and Colloid Science, Springer US, Boston, MA, 2004, pp. 27–81, https://doi.org/10.1007/978-1-4419-9122-5_2.
[40] Y.X.J. Wang, S.M. Hussain, G.P. Krestin, Superparamagnetic iron oxide contrast agents: physicochemical characteristics and applications in MR imaging, Eur. Radiol. 11 (11) (2001) 2319–2331, https://doi.org/10.1007/s003300100908.
[41] X. Yin, S.E. Russek, G. Zabow, F. Sun, J. Mohapatra, K.E. Keenan, M.A. Boss, H. Zeng, J.P. Liu, A. Viert, S.-H. Liou, J. Moreland, Large T1 contrast enhancement using superparamagnetic nanoparticles in ultra-low field MRI, Sci. Rep. 8 (1) (2018) 11863, https://doi.org/10.1038/s41598-018-30264-5.
[42] J.E. Ogbezode, U.S. Ezealigo, A. Bello, V.C. Anye, A.P. Onwualu, A narrative review of the synthesis, characterization, and applications of iron oxide nanoparticles, Discover Nano 18 (1) (2023) 125, https://doi.org/10.1186/s11671-023-03898-2.
[43] V. Sachdeva, A. Monga, R. Vashisht, D. Singh, A. Singh, N. Bedi, Iron oxide nanoparticles: the precise strategy for targeted delivery of genes, oligonucleotides and peptides in cancer therapy, J. Drug Deliv. Sci. Technol. 74 (2022) 103585, https://doi.org/10.1016/j.jddst.2022.103585.
[44] Z. Zhao, M. Li, J. Zeng, L. Huo, K. Liu, R. Wei, K. Ni, J. Gao, Recent advances in engineering iron oxide nanoparticles for effective magnetic resonance imaging, Bioact. Mater. 12 (2022) 214–245, https://doi.org/10.1016/j.bioactmat.2021.10.014.
[45] S.A. Kulkarni, S.-S. Feng, Effects of particle size and surface modification on cellular uptake and biodistribution of polymeric nanoparticles for drug delivery, Pharm. Res. 30 (10) (2013) 2512–2522, https://doi.org/10.1007/s11095-012-0958-3.
[46] H.A. Khan, M.K. Sakharkar, A. Nayak, U. Kishore, A. Khan, 14 - nanoparticles for biomedical applications: an overview, in: R. Narayan (Ed.), Nanobiomaterials, Woodhead Publishing, 2018, pp. 357–384, https://doi.org/10.1016/B978-0-08-100716-7.00014-3.
[47] L. Abarca-Cabrera, P. Fraga-García, S. Berensmeier, Bio-nano interactions: binding proteins, polysaccharides, lipids and nucleic acids onto magnetic nanoparticles, Biomater. Res. 25 (1) (2021) 12, https://doi.org/10.1186/s40824-021-00212-y.
[48] L. Chekli, S. Phuntsho, M. Roy, E. Lombi, E. Donner, H.K. Shon, Assessing the aggregation behaviour of iron oxide nanoparticles under relevant environmental conditions using a multi-method approach, Water Res. 47 (13) (2013) 4585–4599, https://doi.org/10.1016/j.watres.2013.04.029.
[49] M. Mahmoudi, S. Sant, B. Wang, S. Laurent, T. Sen, Superparamagnetic iron oxide nanoparticles (SPIONs): development, surface modification and applications in chemotherapy, Adv. Drug Deliv. Rev. 63 (1) (2011) 24–46, https://doi.org/10.1016/j.addr.2010.05.006.
[50] S. Gao, A. Holkar, S. Srivastava, Protein–polyelectrolyte complexes and micellar assemblies, Polymers 11 (7) (2019) 1097, https://doi.org/10.3390/polym11071097.
[51] J. Sherwood, Y. Xu, K. Lovas, Y. Qin, Y. Bao, Surface functionalization of dopamine coated iron oxide nanoparticles for various surface functionalities, J. Magn. Magn Mater. 427 (2017) 220–224, https://doi.org/10.1016/j.jmmm.2016.10.039.
[52] H. Mettee, A. Asparin, Z. Ali, S. He, X. Li, J. Hall, A. Kim, S. Wu, M.J. Hawker, M. Uchida, H. Wei, Ultrasmall superparamagnetic magnetite nanoparticles as glutamate-responsive magnetic resonance sensors, Sensors 25 (14) (2025) 4326, https://doi.org/10.3390/s25144326.
[53] Y. Zhang, J. Ortiz, S. He, X. Li, B. Kaur, B. Cao, Z. Seiden, S. Wu, H. Wei, Magnetically retrievable nanoparticles with tailored surface ligands for investigating the interaction and removal of water-soluble PFASs in natural water matrices, Sensors 25 (14) (2025) 4353, https://doi.org/10.3390/s25144353.
[54] K. Renault, J.W. Fredy, P.-Y. Renard, C. Sabot, Covalent modification of biomolecules through maleimide-based labeling strategies, Bioconjug. Chem. 29 (8) (2018) 2497–2513, https://doi.org/10.1021/acs.bioconjchem.8b00252.
[55] M. Lahnsteiner, A. Kastner, J. Mayr, A. Roller, B.K. Keppler, C.R. Kowol, Improving the stability of maleimide–thiol conjugation for drug targeting, Chem. Eur J. 26 (68) (2020) 15867–15870, https://doi.org/10.1002/chem.202003951.
[56] M. Gaeta, K. Galletta, M. Cavallaro, E. Mormina, M.T. Cannizzaro, L.R. M. Lanzafame, T. D'Angelo, A. Blandino, S.L. Vinci, F. Granata, T1 relaxation: chemo-physical fundamentals of magnetic resonance imaging and clinical applications, Insights into Imaging 15 (1) (2024) 200, https://doi.org/10.1186/s13244-024-01744-2.

[57] Derrick J. Todd, Anna Kagan, Lori B. Chibnik, Jonathan Kay, Cutaneous changes of nephrogenic systemic fibrosis, Arthritis Rheum. 56 (2007) 3433–3441.
[58] Y. Errante, V. Cirimele, C.A. Mallio, V. Di Lazzaro, B.B. Zobel, C.C. Quattrocchi, Progressive increase of T1 signal intensity of the dentate nucleus on unenhanced magnetic resonance images is associated with cumulative doses of intravenously administered gadodiamide in patients with normal renal function, suggesting dechelation, Investig. Radiol. 49 (10) (2014) 685–690.
[59] S.M. Dadfar, K. Roemhild, N.I. Drude, S. von Stillfried, R. Knüchel, F. Kiessling, T. Lammers, Iron oxide nanoparticles: diagnostic, therapeutic and theranostic applications, Adv. Drug Deliv. Rev. 138 (2019) 302–325, https://doi.org/10.1016/j.addr.2019.01.005.
[60] A. Zhang, K. Meng, Y. Liu, Y. Pan, W. Qu, D. Chen, S. Xie, Absorption, distribution, metabolism, and excretion of nanocarriers *In vivo* and their influences, Adv. Colloid Interface Sci. 284 (2020) 102261, https://doi.org/10.1016/j.cis.2020.102261.
[61] H. Soo Choi, W. Liu, P. Misra, E. Tanaka, J.P. Zimmer, B. Itty Ipe, M.G. Bawendi, J. V. Frangioni, Renal clearance of quantum dots, Nat. Biotechnol. 25 (10) (2007) 1165–1170, https://doi.org/10.1038/nbt1340.
[62] J. Zhang, Y. Ning, H. Zhu, N.J. Rotile, H. Wei, H. Diyabalanage, E.C. Hansen, I. Y. Zhou, S.C. Barrett, M. Sojoodi, K.K. Tanabe, V. Humblet, A. Jasanoff, P. Caravan, M.G. Bawendi, Fast detection of liver fibrosis with collagen-binding single-nanometer iron oxide nanoparticles via T1-Weighted MRI, Proc. Natl. Acad. Sci. 120 (18) (2023) e2220036120, https://doi.org/10.1073/pnas.2220036120.
[63] A. Saraswathy, Shaiju S. Nazeer, N. Nimi, S. Arumugam, Sachin J. Shenoy, Ramapurath S. Jayasree, Synthesis and characterization of dextran stabilized superparamagnetic iron oxide nanoparticles for in vivo MR imaging of liver fibrosis, Carbohydr. Polym. 101 (2014) 760–768, https://doi.org/10.1016/j.carbpol.2013.10.015.
[64] A. Saraswathy, S.S. Nazeer, M. Jeevan, N. Nimi, S. Arumugam, V.S. Harikrishnan, P.R.H. Varma, R.S. Jayasree, Citrate coated iron oxide nanoparticles with enhanced relaxivity for in vivo magnetic resonance imaging of liver fibrosis, Colloids Surf. B Biointerfaces 117 (2014) 216–224, https://doi.org/10.1016/j.colsurfb.2014.02.034.
[65] O. Chen, L. Riedemann, F. Etoc, H. Herrmann, M. Coppey, M. Barch, C.T. Farrar, J. Zhao, O.T. Bruns, H. Wei, P. Guo, J. Cui, R. Jensen, Y. Chen, D.K. Harris, J. M. Cordero, Z. Wang, A. Jasanoff, D. Fukumura, R. Reimer, M. Dahan, R.K. Jain, M. G. Bawendi, Magneto-fluorescent core-shell supernanoparticles, Nat. Commun. 5 (1) (2014) 5093, https://doi.org/10.1038/ncomms6093.
[66] X. Xiao, H. Cai, Q. Huang, B. Wang, X. Wang, Q. Luo, Y. Li, H. Zhang, Q. Gong, X. Ma, Z. Gu, K. Luo, Polymeric dual-modal imaging nanoprobe with two-photon aggregation-induced emission for fluorescence imaging and gadolinium-chelation for magnetic resonance imaging, Bioact. Mater. 19 (2023) 538–549, https://doi.org/10.1016/j.bioactmat.2022.04.026.
[67] W. Pan, M. Rafiq, W. Haider, Y. Guo, H. Wang, M. Xu, B. Yu, H. Cong, Y. Shen, Recent advances in NIR-II fluorescence/photoacoustic dual-modality imaging probes, Coord. Chem. Rev. 514 (2024) 215907, https://doi.org/10.1016/j.ccr.2024.215907.
[68] N. Insin, J.B. Tracy, H. Lee, J.P. Zimmer, R.M. Westervelt, M.G. Bawendi, Incorporation of iron oxide nanoparticles and quantum dots into silica microspheres, ACS Nano 2 (2) (2008) 197–202, https://doi.org/10.1021/nn700344x.
[69] O. Chen, H. Wei, A. Maurice, M. Bawendi, P. Reiss, Pure colors from core–shell quantum dots, MRS Bull. 38 (9) (2013) 696–702, https://doi.org/10.1557/mrs.2013.179.
[70] S. Kuang, Y. Wan, Y. Dai, C. Mo, Y. Fei, J. Shi, C. Han, T. Huang, Multifunctional molecular Theranostic agent for fluorescence-magnetic resonance dual-modal imaging and photodynamic-chemodynamic synergistic therapy, Sensor. Actuator. B Chem. 426 (2025) 137035, https://doi.org/10.1016/j.snb.2024.137035.
[71] M. Zhang, W. Wang, F. Wu, P. Yuan, C. Chi, N. Zhou, Magnetic and fluorescent carbon nanotubes for dual modal imaging and photothermal and chemo-therapy of cancer cells in living mice, Carbon 123 (2017) 70–83, https://doi.org/10.1016/j.carbon.2017.07.032.
[72] R.J. Wydra, P.G. Rychahou, B.M. Evers, K.W. Anderson, T.D. Dziubla, J.Z. Hilt, The role of ROS generation from magnetic nanoparticles in an alternating magnetic field on cytotoxicity, Acta Biomater. 25 (2015) 284–290, https://doi.org/10.1016/j.actbio.2015.06.037.
[73] M.S. Valic, M. Halim, P. Schimmer, G. Zheng, Guidelines for the experimental design of pharmacokinetic studies with nanomaterials in preclinical animal models, J. Contr. Release 323 (2020) 83–101, https://doi.org/10.1016/j.jconrel.2020.04.002.
[74] M.P. Monopoli, D. Walczyk, A. Campbell, G. Elia, I. Lynch, F. Baldelli Bombelli, K. A. Dawson, Physical−Chemical aspects of protein Corona: relevance to in vitro and in vivo biological impacts of nanoparticles, J. Am. Chem. Soc. 133 (8) (2011) 2525–2534, https://doi.org/10.1021/ja107583h.
[75] V.C. Ferreira-Filho, B. Morais, B.J.C. Vieira, J.C. Waerenborgh, M.J. Carmezim, C. N. Tóth, S. Même, S. Lacerda, D. Jaque, C.T. Sousa, M.P.C. Campello, L.C.J. Pereira, Influence of SPION surface coating on magnetic properties and Theranostic profile, Molecules 29 (8) (2024) 1824, https://doi.org/10.3390/molecules29081824.